In vitro and *in vivo* studies on nanocrystalline Ti fabricated by equal channel angular pressing with microcrystalline CP Ti as control

F. L. Nie,[1,2] Y. F. Zheng,[1,3] S. C. Wei,[3,4] D. S. Wang,[5] Z. T. Yu,[6] G. K. Salimgareeva,[7] A. V. Polyakov,[7] R. Z. Valiev[7]

[1]State Key Laboratory for Turbulence and Complex System and Department of Materials Science and Engineering, College of Engineering, Peking University, Beijing 100871, China
[2]Center for Medical Device Evaluation, SFDA, Beijing 100044, China
[3]Center for Biomedical Materials and Tissue Engineering, Academy for Advanced Interdisciplinary Studies, Peking University, Beijing 100871, China
[4]Center for Biomaterials and Medical Devices, School of Stomatology, Peking University, Beijing 100081, China
[5]Institute of Stomatology, Chinese PLA General Hospital, Beijing 100853, China
[6]Biomaterials Research Center, Northwest Institute for Nonferrous Metal Research, Xian 710016, China
[7]Institute of Physics of Advanced Materials, Ufa State Aviation Technical University, Ufa, Russia

Abstract: Bulk nanocrystalline Ti bars (Grade 4, $\Phi 4 \times 3000$ mm^3) were massively fabricated by equal channel angular pressing (ECAP) via follow-up conform scheme with the microcrystalline CP Ti as raw material. Homogeneous nanostructured crystals with the average grain size of 250 nm were identified for the ECAPed Ti, with extremely high tensile/fatigue strength (around 1240/620 MPa) and adorable elongation (more than 5%). Pronounced formation of bone-like apatite for the nanocrystalline Ti group after 14 days static immersion in simulated body fluids (SBF) reveals the prospective *in vitro* bioactive capability of fast calcification, whereas an estimated 17% increment in protein adsorption represents good bioaffinity of nanocrystalline Ti. The documentation onto the whole life circle of osteoblast cell lines (MG63) revealed the strong interactions and superior cellular functionalization when they are co-incubated with bulk nanocrystalline Ti sample. Moreover, thread-structured specimens were designed and implanted into the tibia of Beagles dogs till 12 weeks to study the *in vivo* responses between bone and metallic implant made of bulk nanocrystalline Ti, with the microcrystalline Ti as control. For the implanted nanostructured Ti group, neoformed bone around the implants underwent the whole-stage transformation proceeding from originally osteons or immature woven bone to mature lamellar bone (skeletonic trabecular), even with the remodeling being finished till 12 weeks. The phenomenal osseointegration of direct implant-bone contact can be revealed from the group of the ECAPed Ti without fibrous tissue encapsulation in the gap between the implant and autogenous bone. © 2012 Wiley Periodicals, Inc. J Biomed Mater Res Part A: 00A: 000–000, 2012.

Key Words: bulk nanocrystalline Ti, equal channel angular pressing, bioactivity, bone growing, remodeling

How to cite this article: Nie FL, Zheng YF, Wei SC, Wang DS, Yu ZT, Salimgareeva GK, Polyakov AV, Valiev RZ. 2012. *In vitro* and *in vivo* studies on nanocrystalline Ti fabricated by equal channel angular pressing with microcrystalline CP Ti as control. J Biomed Mater Res Part A 2012:00A:000–000.

INTRODUCTION

Since the first case of clinical surgery documented,[1] over 30 years ago, commercially pure Ti (CP Ti) has been approved as one component of medical devices by ASTM trials and FDA clinics. At present, CP Ti is widely used as endosseous prosthesis in orthopedics (e.g., metatarsophalangeal joint implant, aneurysm clips, thyroplasty and trauma) and dentistry (e.g., dental implant and mandibular restoration) owing to its excellent biocompatibility and corrosion resistance.[2] Nevertheless, the unfavorable mechanical behavior such as insufficient strength and excess modulus of CP Ti limit its application to nonload bearing devices due to the stress shielding effect. The bioinert surface of CP Ti is another barrier for implantation loosening due to the gap between preferentially formed fibrous tissue and the fresh implant, instead of the desired effect of direct Ti-bone bonding or osseointegration.[3] Many methods such as alloying,[4] new phase modulation,[5] surface nanotopography,[6] even surface modifications with bio-glasses/ceramics such as hydroxyapatite (HA) coating,[7] bone morphogenetic protein

(BMP), or collagen grafting[8] were tried to physically strengthen or biologically enhance the bio-function of CP Ti, but unfortunately new problems came out including adverse effects derived from nonfriendly elements or overdose, interfacial bonding mismatch, low efficiency even instability failure due to the fast degradation of coating by proteinases under *in vivo* condition.

Recently developed approaches for effectively enhancing the mechanical and fatigue properties of CP Ti through grain refinement and nanostructuring by severe plastic deformation (SPD) techniques[9] may offer a new chance to solve the problem mentioned above. The new SPD processing method, namely equal channel angular pressing (ECAP) with follow-up drawing and annealing can maximize the sizable products up to 3000 mm in length and 4–8 mm in diameter, with h8 tolerance[10] and bending no more than 2 mm per meter.[11–13] The bulk samples with nanocrystalline microstructure ensure the cornerstone of industrialization of bulk nanostructured materials for its biomedical application[11] with following advantages. First, expensive (and as a rule, toxic) alloying elements can be avoided because the required strength would be achieved by nanostructuring. Second, high strength of bulk nanocrystalline Ti allows size reduction of the individual implanted device while maintains the same biomechanics, which lowers the trauma area of surgical and favors minimally invasive surgery. Third, in comparison to the surface nanocoated Ti, the uniform feature of all bulk nanostructure without interfaces guarantee the integrated property as a whole body. Although some *in vitro* studies on the appealing biological behavior recently had been published,[11,14–17] there is no report on the *in vivo* study of the bulk nanocrystalline Ti processed by SPD till now.

In this article, not only the material characterizations of the ECAP-processed titanium (the ECAPed Ti), but also the interactions between bone and ECAPed Ti implants had been undertaken. 20 Beagles were adopted to serve as the host in order to minute the long-term bone-implant contact, from 1 week to 12 weeks. Histomorphometry and immuno-histochemistry analysis on the different titanium implants with nano/microcrystalline grain sizes were conducted and compared to reveal the situations of bone growth and remodeling, via the method of colorimetry-based assays, immunohistochemical staining, image analyzing, and micro computed-tomograph (CT) scanning.

MATERIALS AND METHODS
Materials preparation
Microcrystalline CP Ti (Grade 4) and corresponding nano-crystalline Ti produced by ECAP-conform with drawing was investigated. Experimental samples (disc shape with the bulk size of $\Phi 4 \times 1$ mm^3) for *in vitro* study were mechanically polished up to 2000 grit, ultrasonically cleaned in acetone, absolute ethanol and distilled water in sequence, and then dried in open air. For the cytotoxicity test extraction preparation, all experimental samples were sterilized by autoclave at 121°C for at least 30 min. For those specimens in animal study, peri-implant size of $\Phi 4 \times 7$ mm^3 by turning

machining was applied in the threaded cylindrical shape. Before they were implanted into the animals, samples sterilization was guaranteed after overnight Gamma radiation by 5 Gy.

Materials characterization
X-ray diffractometer (Rigaku DMAX 2400) using Cu Kα radiation was employed for the identification of the constitutional phases. Transmission electron microscopy (TEM) bright field image by JEM 200CX under 120 kV was performed to reveal the grain/subgrain size distributions and microstructure observations of the experimental samples, after standard grinding, polishing, and dimpling procedures by 2 h ion thinning.

The surface wettability was assessed by measuring the contact angle of distilled water. Tests of contact angles were conducted by the sessile-drop method with a contact angle system (CAS, Data physics OCA20) at the ambient temperature.

The miniature monitoring and roughness of naked surface from CP Ti and the ECAPed Ti samples were recorded by atomic force microscopy (AFM, SPI 3800N) scanning. The dimensions of the explored zone were 5×5 μm^2 and triplicated measurements were done for each group of samples.

In-vitro HA and protein adsorption
Calcification and HA deposition were identified on the top surface of experimental samples after their standard soaking in simulated body fluid (SBF). The immersion test was carried out in SBF with the ratio of solution to sample surface 20 mL/cm^2 according to ASTM-G31-72[18] and the temperature was kept at 37°C by water bath. After 1, 3, 7, and 14 days, the samples were removed from the given solution, gently rinsed with distilled water, and quickly dried and kept in a drying oven at room temperature. The surface monitoring of the samples before and after immersion were characterized by environmental scanning electron microscopy (ESEM, AMRAY-1910FE). The surface change of chemical composition of experimental samples was analyzed by EDS and XPS (AXIS Ultra, Kratos).

For the protein adsorption assay, bovine serum albumin (BSA, Baosai Biotechnology Inc., Beijing) was used as a standardized model protein. One hundred microliters of protein solution (0.2 mg/mL protein/saline) was pipetted onto the surface of the experimental substrate, with the tissue culture plate as negative control and saline as blank. After incubation for 2, 4, and 24 h at 37°C, nonadherent proteins were removed and mixed with micro-bicinchoninic acid (BCA) at 37°C for 30 min. The amount of the removed albumin, as well as the total amount of albumin, was quantified using a microplate reader at 570 nm.

Cell culture
Murine fibroblast cell lines (L-929), osteoblast cell lines (MG63), vascular smooth muscle cells (VSMC) and endothelial cells (ECV304) were adopted here to evaluate the cytotoxicity in an indirect way, while MG63 was co-cultured

with the sample substrates to demonstrate the long-term interactions between the cells and samples of CP Ti and the ECAPed Ti. All the cells were incubated in Dulbecco's modified Eagle's medium (DMEM), mixed with 10% fetal bovine serum (FBS), 100 U mL^{-1} penicillin and 100 µg mL^{-1} streptomycin at 37°C in a humidified atmosphere of 5% CO_2.

Cell attachment and spread. Initial attachment of MG63 cells was assessed by measuring the amount of cells (via both way of SEM imaging and ELISA kit) attached onto substrates of the samples after 4 and 24 h of incubation. Then, PBS was used to remove the nonadherent cells. The adhered cells were fixed in 2.5% glutaraldehyde solutions for 1 h at room temperature followed by dehydration in a gradient ethanol/distilled water mixture (from 50% till 100%) for 10 min each. Cell spread status on the surface in the early stage is also based on the tallying and imaging.

Cytotoxicity and proliferation. The cytotoxicity tests were carried out by indirect and direct contact. For the indirect way, extracts were prepared using DMEM serum-free medium as the extraction medium with the surface area of extraction medium ratio 3 cm^2/mL^{19} in a humidified atmosphere with 5% CO_2 at 37°C for 72 h. The control groups involved the use of DMEM medium as negative control and DMSO as positive control. Cells were incubated in 96-well cell culture plates at 5×10^3 cells/100 µL medium in each well and incubated for 24 h to allow attachment. The medium was then replaced with 100 µL of extracts. After incubating the cells in a humidified atmosphere with 5% CO_2 at 37°C for 1, 2, and 4 days, respectively, the 96-well cell culture plates were observed under an optical microscope. After that, 10 µL MTT was added to each well. The samples were incubated with MTT for 4 h at 37°C, then 100 µL formazan solubilization solution (10% SDS in 0.01M HCl) was added in each well overnight in the incubator in a humidified atmosphere. For the direct way, cells were directly seeded on the sterilized substrates in the 96-well plate. The spectrophotometrical absorbance of the samples was measured by microplate reader (Bio-RAD680) at 570 nm with a reference wavelength of 630 nm.

Cell differentiation and mineralization. Alkaline phosphatase (ALP) activity of osteoblasts was examined at 3, 7, 14, and 21 days using colorimetry-based assays. Cells were seeded onto the sample substrate in a 96-well plate and washed twice with PBS when it's on time, and incubated with solution of 200 µL 0.2% Triton to undergo the lysis reaction. After 30 min, 100 µL supernatant was pipetted separated into 5 wells in a new 96-well plate, one of which was to assess the total amount of protein via BCA kit under instruction. A 200 µL mixture of 50 parts A and 1 part B was added into the well and co-incubated in a humidified atmosphere with 5% CO_2 at 37°C for 30 min. Then the microplate was measured at 570 nm to reveal the amount of protein. For ALP colorimetry of the other 4 wells respectively, an addition of 100 µL mixed working solution for 45 min, which consisted of 100 µL 0.1 mM p-Nitrophenylphosphate, 1 mL 1M $MgCl_2$ and balanced carbonate buffer within 10 mL. Eventually, 25 µL 1M NaOH was added to stop the reaction. ALP activity was evaluated as the amount of nitrophenol released through the enzymatic reaction and measured at 405 nm using an ELISA reader (Bio-RAD680).

To quantify matrix mineralization, the Alizarin Red S-stained (50% ethanol and 1% Alizarin Red S with pH 6.0, Sigma-Aldrich) cultures were incubated with 100 mM cetylpyridinium chloride for 1 h to solubilize. The absorbance of released calcium-bound Alizarin Red was measured at 570 nm.

Animal Test

Animal preparation. Twenty female Beagle dogs ordered from Vital River Laboratories, 12 months of age and around 10 kg in weight, were involved in the study. The study was approved by the Institutional Animal Care and Use Committee (IACUC) and experimented in the Laboratory Animal Center (LAC) of Peking University, China (approval No. 621.2531.31-14-01). The dogs were well fed and carefully observed for a week in LAC before the implantation trial, and they were randomly divided into five groups.

Surgical process. Animals were aseptically cleaned and anesthetized with 1 mL/kg pentobarbital solution delivered into ear vein, and additional primacaine™ was injected as needed local anaesthetic. After their legs were shaved and scrubbed with 10% providoneiodine solution, the surgical site was exposed via skin incision and muscle dissection. Threaded samples of the nanocrystalline ECAPed Ti were implanted into the tibia of the right rear leg after drilling a suited hole in the flat area, while the implantation site of microcrystalline CP Ti was located in the corresponding left side tibia. Profuse irrigation with sterile physiological saline was used for cooling and cleaning. Muscle and skin were sutured separately with suture thread. Certain antibiotics were injected after operation in order to avoid the infections. Tetracycline and calcium were individually marked as the new bone formation via intravenous injection at 2 and 4 weeks after surgery. Threaded cylindrical samples of the ECAPed Ti implanted into the tibia of Beagle dogs were harvested 1, 2, 4, 8, and 12 weeks ($n = 4$) after surgery. The IACUC from Peking University approved this protocol and all experimentation was performed in accordance with the guidelines of animal research.

Histomorphometry analysis. The tibia containing the screw-like titanium implants was harvested and fixed in 10% buffered formalin for 2 weeks at 4°C. Specimens were dehydrated in an ascending series of alcohol rinses and embedded in light-curing epoxy resin without decalcification. Embedded specimens were sawed perpendicular to the longitudinal axis of the cylindrical implants at a site 0.5 mm from the apical end of the implant. Specimens were ground to a thickness of 30 mm with a grinding system. Sections were immunohistochemical stained with toluidine blue, and observed via optical microscope (Olympus IX71, Japan).

Micro-CT scanning and 3D reconstruction. After the animals were sacrificed, the tibia including the implants was harvested; excess tissue was removed and immediately fixed in 10% neutral buffered formalin solution. Prior to scanning, bone blocks containing only one implant each, were dehydrated in ethanol 70% to prevent drying during scanning. For a quantitative 3D analysis, the specimens were placed vertically onto the sample holder of a micro-CT imaging system, Skyscan 1072 desktop X-ray Micro-tomography System (Skyscan, Kontich, Belgium), with the long axis of the implant perpendicular to the scanning beam. Subsequently, a high resolution scan was recorded at 18-μm-voxel resolution. Then, a serial of affiliated software including CTAn V1.7, NRecon V1.4, and CTVol V1.11 (SkyScan, Kontich, Belgium) was performed on the projected files to obtain the final 3D-reconstruction images and derived parameters.

Haemocompatibility assessment

Hemolysis tests. Healthy human blood containing sodium citrate (3.8 wt %) in the ratio of 9:1 was taken and diluted with normal saline (4:5 ratio by volume). Microcrystalline CP Ti and the nanocrystalline ECAPed Ti were dipped in a standard tube containing 10 mL of normal saline that were previously incubated at $37°C$ for 30 min. Then 0.2 mL of diluted blood was added to this standard tube and the mixtures were incubated for 60 min at $37°C$.[19] Similarly, normal saline solution was used as a negative control and deionized water as a positive control. After this period, all the tubes were centrifuged for 5 min at 3000 rpm and the supernatant was carefully removed and transferred to the cuvette for spectroscopic analysis at 545 nm. In addition, the hemolysis was calculated using an ultraviolet spectrophotometer (UNIC-7200, China). The hemolysis was calculated based on the average of three replicates.

$$Hemolysis = \frac{OD(test) - OD(negative\ control)}{OD(positive\ control) - OD(negative\ control)} \times 100\%$$

Platelet adhesion. Platelet-rich plasma (PRP) was prepared by centrifuging the whole blood for 10 min at a rate of 1000 rpm/min. The PRP was overlaid atop the experimental alloys plates and incubated at $37°C$ for 1 h. The samples were rinsed with PBS to remove the nonadherent platelets. The adhered platelets were fixed in 2.5% glutaraldehyde solutions for 1 h at room temperature followed by dehydration in a gradient ethanol/distilled water mixture (from 50% till 100%) for 10 min each and dried in hexamethyldisilazane (HMDS) solution.[20] The surface of platelet attached experimental alloy sheets were observed by ESEM. Different fields were randomly counted and values were expressed as the average number of adhered platelets per $μm^2$ of surface.

Statistical analysis

All experiments were performed at least three times, data averaged and expressed as mean $\pm$ standard deviation (SD). Statistical analysis was performed using one-way analysis of variance (ANOVA) and significance was considered at $p \leq 0.05$.

RESULTS

In vitro assessment of the ECAPed Ti

Materials characterizations and mechanical behaviors.
Figure 1(a) shows the TEM image and the grain size distribution of the bulk nanocrystalline ECAPed Ti. Under the bright field observation and the statistics calculation from the histogram, it is clearly seen that the average grain size of the ECAPed Ti is about 250 nm, way smaller than that of 10–30 μm as the original grain size of the microcrystalline CP Ti control reported by the present authors.[21,22] Correspondingly alpha-Ti with hcp structure can be clearly demonstrated according to the typical Bragg peaks at featured degrees (for example, 36°, 39.6°, and 76°) in Figure 1(b). The surface roughness and wettability of experimental samples were measured and shown in Figure 1(c,d). Top-view surface feature displays a less rough topography of the ECAPed Ti, and the value of average roughness (Ra) varies from 119.70 $\pm$ 18.93 nm to 58.13 $\pm$ 8.72 nm for CP Ti and the ECAPed Ti in a significant way by the area of 5 × 5 $μm^2$. The values of root mean squared (RMS) microroughness and P-V macroroughness are also listed to show a specific characterization, from which much lower microroughness is obtained for the ECAPed Ti. As for surface wettability, enhanced hydrophilicity with a lower contact angle (42.58 $\pm$ 1.43°) exists for the ECAPed Ti compared with that of original CP Ti (46.93 $\pm$ 2.12°).

Table I displays the mechanical properties of CP Ti and the ECAPed Ti after the tensile tests under the ambient temperature. The refinement of grains brings about significant enhancement of strength for CP Ti, as can be seen that the yield strength of nanocrystalline ECAPed Ti increases by 100% (559MPa vs. 1190 MPa) and the ultimate tensile strength increases by 70% (712 MPa vs. 1240 MPa). The separate data in rupture strength and elongation does not exceed 3%, which reveals that the formed nanostructure is homogeneous within the body of the ECAPed Ti. Instead of the typical strength-ductility behavior induced by conventional rolling or drawing, the ductility of the ECAPed Ti goes down in comparison to that of CP Ti, but remains up to 10%, which is still sufficient as bone implants.

Bonelike apatite formation and protein adsorption on the substrate of the ECAPed Ti. Figure 2 shows the surface morphologies under SEM after 3 and 14 days static immersion in SBF. There was no apparent observation of Ca-P deposition on the surface of CP Ti group in the first several days, with only a few particle sediments appearing in the high-magnification image after 14 days immersion [Fig. 2(c)]. While for the group of the ECAPed Ti, the aggregation of some rounded nodulus started to emerge on the surface after 3 days soaking. After 14 days immersion, bonelike apatite coatings were identified by means of EDS (with an approximate Ca/P ratio of 1.67) and substantially found on the ECAPed Ti as revealed in Figure 2(d).
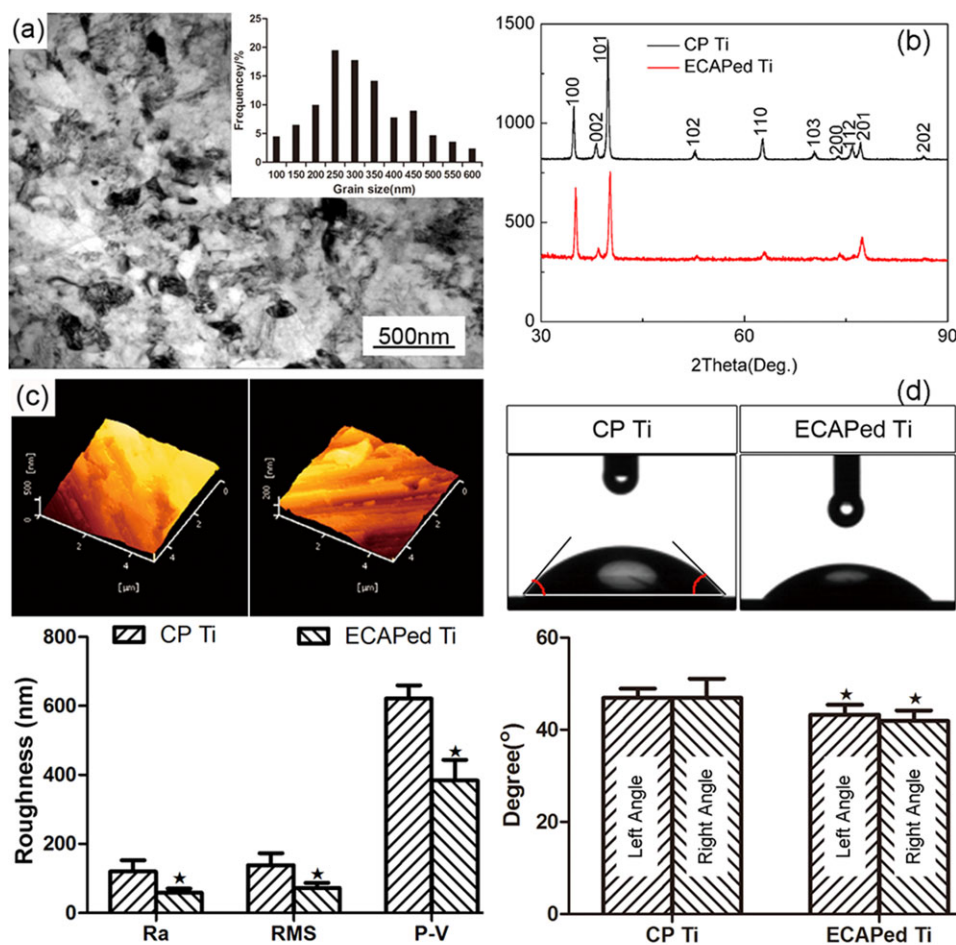
FIGURE 1. Materials characterization of (a) TEM image of the ECAPed Ti in bright field; (b) XRD patterns of CP Ti and the ECAPed Ti; surface monitoring of (c) profilometric roughness and (d) surface wettability of CP Ti and the ECAPed Ti. The inset in (a) represents the histogram of grain size distribution from the TEM bright field image. *Significant against cell proliferation on control group at $p \leq 0.05$. [Color figure can be viewed in the online issue, which is available at wileyonlinelibrary.com.]

A nonspecific protein named albumin was adopted to evaluate the general protein adsorption as bioaffinity. Figure 3 illustrates the adhesion of albumin on top of experimental samples within the initial 24 h. Within the first 2 h, the plot of BSA adsorption keeps ascending quickly with the passage of time, then gets temporarily saturated at 4 h and finally reaches the top till 24 h for CP Ti, the ECAPed Ti and the tissue culture plate (as blank group). It can be clearly seen that BSA adsorption onto the substrate of the ECAPed Ti (73.64% at 24 h) throughout the test dominates well above the tissue culture plate and CP Ti groups (64.01% and 56.02% at 24 h).

Cellular responses, osteoblasts interactions, and haemocompatibility onto the ECAPed Ti. By way of indirect method, the proliferation viability of four different cell lines till 4 days' incubation was shown in Figure 4. For fibroblast cells (L929), although the cell viability increases all the time for both CP Ti and the ECAPed Ti groups, a significant growth lag can be seen among cells for negative control and the other experimental groups. For osteoblast-like cells (MG 63), cells grow very well and a comparable proliferation ration can be found for both CP Ti and ECAPed Ti groups during the whole period, even at an equivalent level with the negative control. In Figure 4(c), vascular smooth muscle

TABLE I. Mechanical Properties of Pure Ti Before and After SPD Treatments

Samples	σ_{UTS}, MPa	$\sigma_{0.2}$, MPa	δ, %	ψ, %	FS, MPa
CP Ti (certificate data)	712.0 ± 17.0	559.5 ± 41.7	26.0 ± 1.4	49.5 ± 3.5	340 ± 22.3
ECAPed Ti	1240 ± 116.4	1190 ± 14.1	11.5 ± 0.7	45.5 ± 5.0	620 ± 50.8

σ_{UTS} stands for ultimate tensile strength, $\sigma_{0.2}$ for yielding stress, δ for elongation, and ψ for reduction of area; FS stands for fatigue strength, which refers to the mechanical strength at 10^6 cycles.
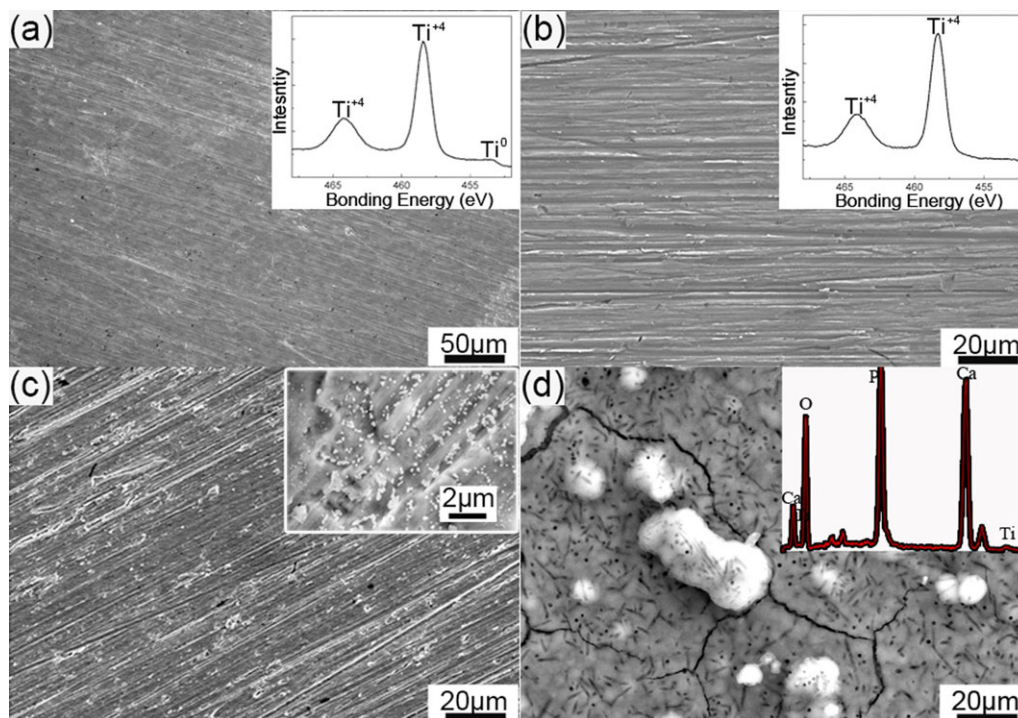
FIGURE 2. Bonelike apatite formation ability: SEM observations of morphologies onto the substrate of (a), (c) as CP Ti and (b), (d) as ECAPed Ti after immersion in SBF. (a) and (b) refers to 3 days immersion; (c) and (d) for 14 days. The inset in (a) and (b) stands for the high-resolution XPS spectra of the naked substrates from CP Ti and the ECAPed Ti, respectively, before the immersion test. The inset in (c) denotes the higher-magnification image, and the inset in (d) shows the EDS pattern. [Color figure can be viewed in the online issue, which is available at wileyonlinelibrary.com.]

cells (VSMC) in the experimental sample groups did not proliferate as well as that in the negative control from the first day culture till the end. While for ECV304, a similar situation occurs in the cell viability as that in MG63. A whole life circle of osteoblast involving cell spread, attachment, differentiation and mineralization was evaluated via biochemistry reagent kit and showed in Figure 5. Talking about the cell adhesion and spread in Figure 5(a), substantial attached MG63 cells (2.09×10^4 cells/cm^2 for the ECAPed Ti group) can be evidently detected as they spread out, exhibiting spindle-shaped within 24h. A higher amount of cell community occurs for the ECAPed Ti group since the early stage (at 40 min incubation), revealed either by cell counting or enzyme-linked method. In the follow-up growing period, MG63 cells favorably proliferate when directly co-cultured with the ECAPed Ti sample and excels over the CP Ti group and the negative control group, especially in the 7 days cultivation [with the viability of 129.5% v.s. 108.5% in Fig. 5(b)]. In terms of cell differentiation, the ALP activity for the ECAPed Ti group (0.0447 ± 0.001, 0.076 ± 0.010, and 0.167 ± 0.003 nmol/min/μg protein for 7, 14, and 21 days, respectively) demonstrates much promoted expression and developing activity over that of CP Ti group. After 21 days cell culture, matrix mineralization on the ECAPed Ti group shows a slightly higher alizarin red release than that of CP Ti group either.

Both the hemolysis rates for the ECAPed Ti and CP Ti samples stay much lower than 5%, as illustrated in Figure 6(a), which is regarded as a biosafety threshold and stands for well-behaved haemocompatibility. The number of

adhered platelets seemed to be similar for the ECAPed Ti and CP Ti groups, while the shape and activation status of the platelets behaves dramatically in a different way. For CP Ti group, a cluster of positive platelets with long pseudopodia were actively scattered, as shown in Figure 6(c). While round- and smooth-shaped platelets were attached on the surface of the nanostructured ECAPed Ti group.

In vivo biological investigations on bone growth around the ECAPed Ti

Histomorphometry analysis and histomorphology observations. In order to understand the nature of interfacial responses between bone and peri-implant made by bulk
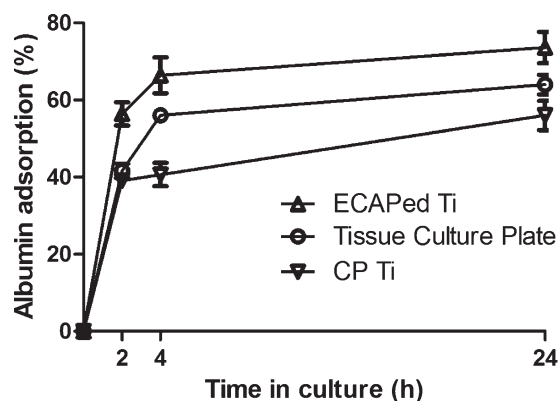

FIGURE 3. Bioaffinity evaluation of the protein adsorption of CP Ti, the tissue culture plate and the ECAPed Ti.
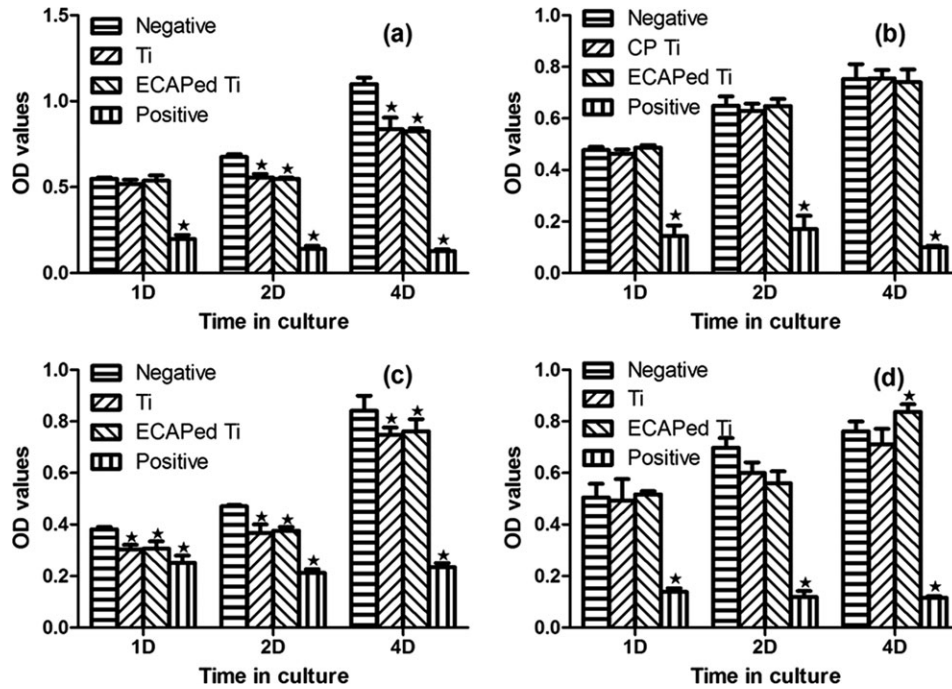
FIGURE 4. Cell proliferations of (a) L929; (b) MG63; (c) VSMC; and (d) ECV304 in an indirect way. *Significant against cell proliferation on control group at $p \leq 0.05$.

nanostructured Ti, a pilot study of animal experiment was carried out. Figure 7 shows the parameters of bone mineral density (BMD) and bone volume/tissue volume (BV/TV) around the implant till 12 weeks derived from micro-CT

reconstruction and analysis. In the case of the ECAPed Ti group, BMD keeps growing fast in the first few weeks as shown in Figure 7(a). After 4 weeks, it starts to get declined as time increases. However this fall occurs at 8 weeks for
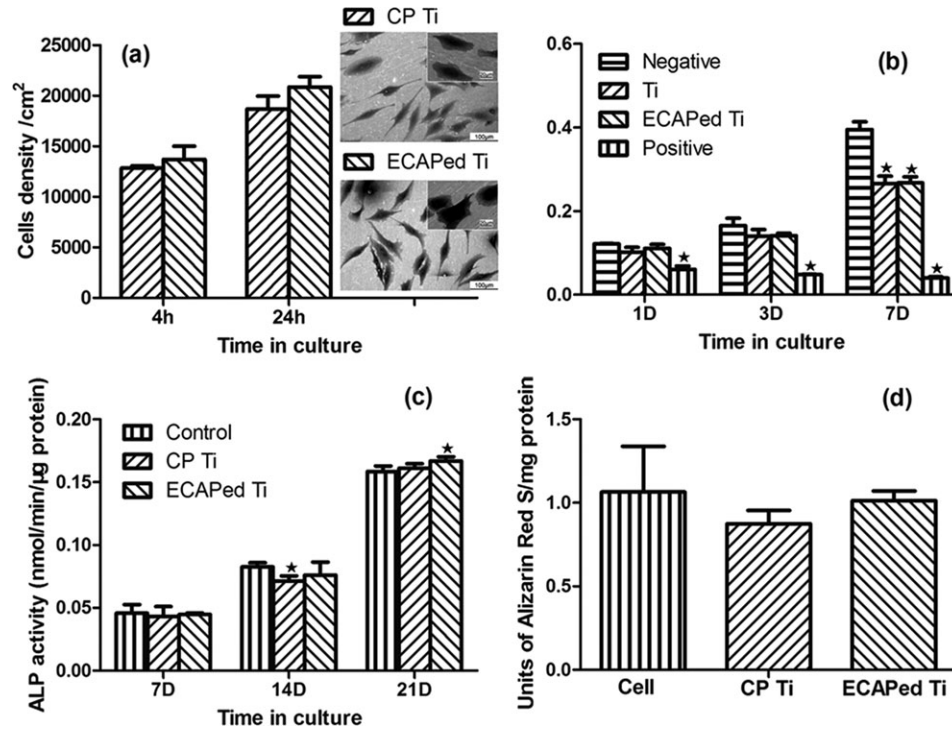

FIGURE 5. Cellular interactions of osteoblast cell lines: (a) Cell attachment and spread of MG63 within 24 h and (b) cell viability and proliferation till 7 days by means of cell-substrates coincubation assay; the follow-up cellular functionalization expression of (c) ALP activity and (d) cell mineralization on the substrate of CP Ti and the ECAPed Ti. Insets in (a) are SEM observations of MG 63 on substrates. *Significant against cell proliferation on control group at $p \leq 0.05$.
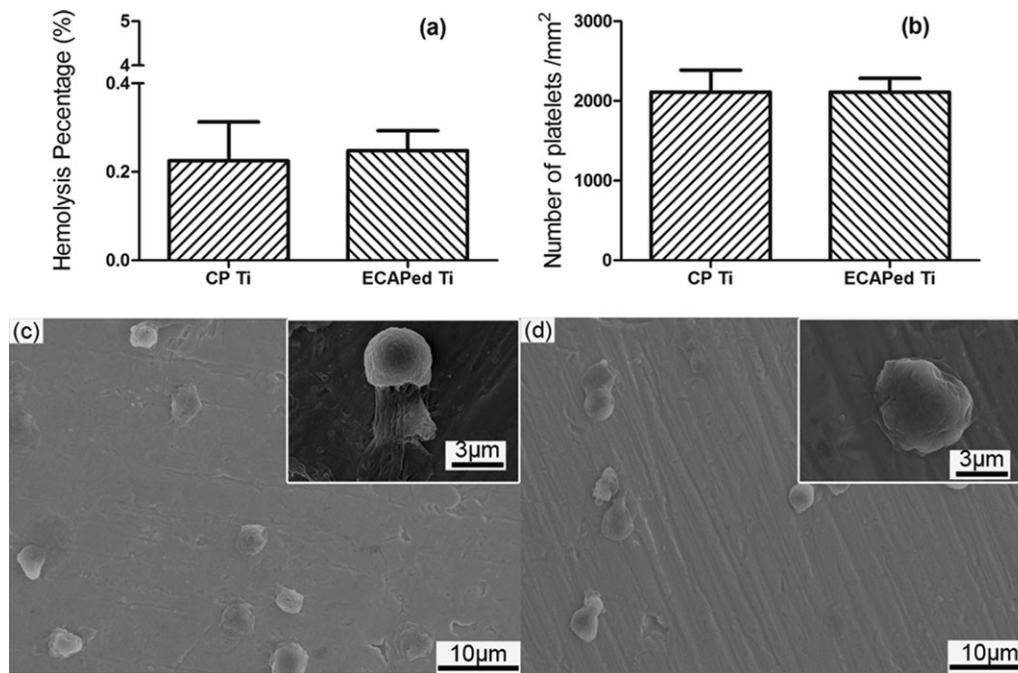
FIGURE 6. Haemocompatibility assessment of (a) hemolysis rate; (b) number of adhered platelets; the SEM observation of adhered platelets onto the surface of (c) CP Ti and (d) ECAPed Ti.

the CP Ti group. Meanwhile, a remarkably higher amount of BMD around the ECAPed Ti implant can be clearly revealed in comparison to that around CP Ti implant at the site of cancellous bone in the first few weeks. Especially at 4 weeks harvest postoperatively this gap reaches the maximum, that is, 0.675 ± 0.022 versus 0.524 ± 0.015 g/cm^3. No such obvious discrepancy can be obtained after 8 weeks between two experimental groups. Similarly, the percentage of BV/TV around the ECAPed Ti implant in Figure 7(b) takes up an exceeded occupation over that from CP Ti at 4 weeks after surgery ($74.91 \pm 2.7\%$ vs. $69.80 \pm 2.5\%$) in a significant way ($p \leq 0.05$).

Figure 8 shows the histological image of new bone around the CP Ti and the ECAPed Ti implants at first 2 weeks with immunohistochemical staining. In the dyeing image of histotomy, dark blue area represents the newly formed bone and normal blue stands for the original bone

(or called autogenous bone). At the first week as shown in Figure 8(a,b), it can be seen that a lot of osteocytes aggregate together and so-called new bone starts to come into being in the darker blue area between the black implant and blue autogenous bone. Apart from the substantial emerge of new bone in the cancellous bone zone, a much thicker layer of such spindle-like woven bone with less density and light color could be detected in outmost of the original bone in Figure 8(b). Some of them even stretched out onto the gap or surface around the implant thread. In 2 weeks postoperatively, the growth of new bone in the case of the ECAPed Ti group was overwhelmingly evident with the evolutionary change of the shape and density of the fresh bone as shown in Figure 8(d,e). The periphery thickness of new bone in the the ECAPed Ti group was largely increased than that at the first week, at the same time exceeded that of the CP Ti group, as denoted by the red
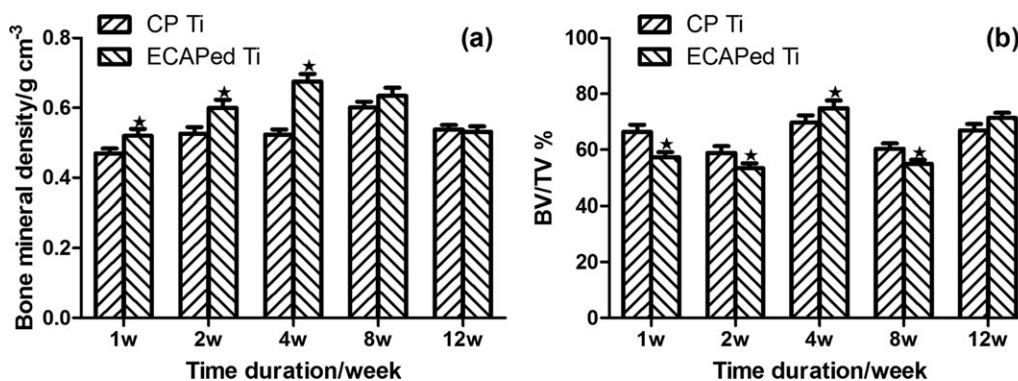

FIGURE 7. Outcomes of (a) BMD and (b) BV/TV from 3D reconstructive after micro-CT analysis. *Significant against cell proliferation on control group at $p \leq 0.05$.
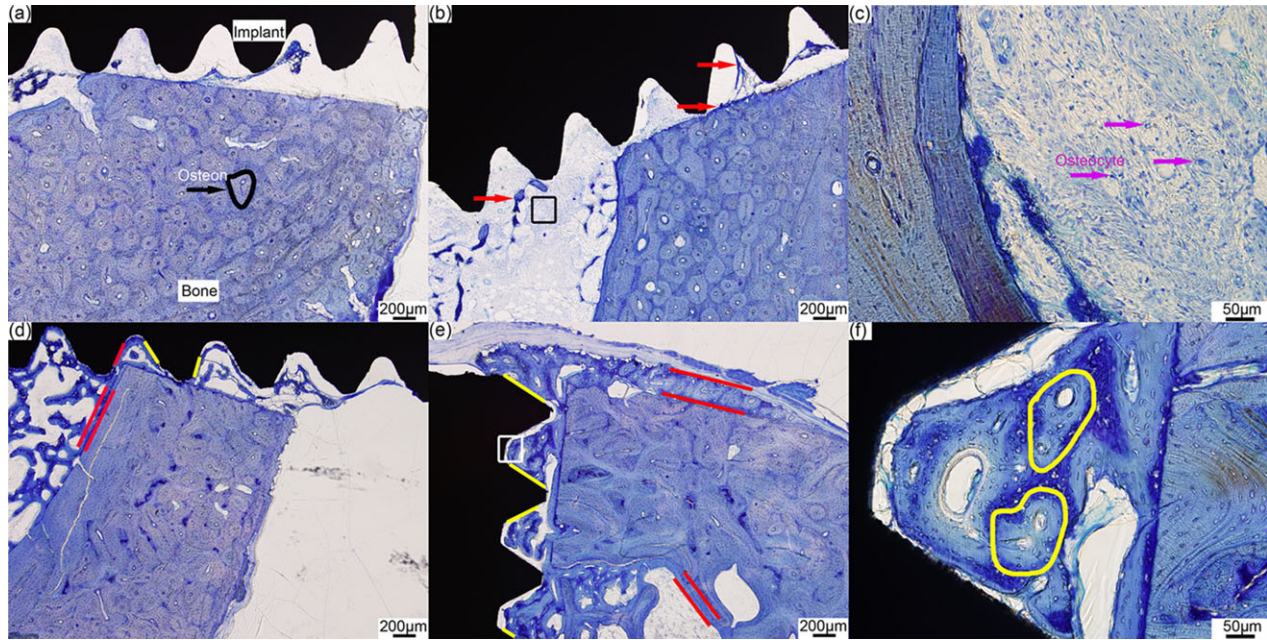
FIGURE 8. Histotomy of bone contact immunostained by toluidine blue at 1 weeks of (a), (b), (c) and 2 weeks of (d), (e), (f) postoperatively. (a) and (d) refers the CP Ti implant; (b) and (e) refers the ECAPed Ti implant; while (c) and (f) refers to the higher-magnification images of (b) and (e), in the area of the black hollow square. Black arrow and loop in (a) refers to osteon, the unit cell of the bone. Red arrows in (b) refers to the newly-formed woven bone. Dot-like spot in blue in (c) refers to the osteocytes. Red line in (d) and (e) shows the boundary and the gap of the newly formed bone. Yellow line in (d) and (e) refers to the bone-implant contact, one major symbol of osseointegration. [Color figure can be viewed in the online issue, which is available at wileyonlinelibrary.com.]

parallel line. Checking the area near the thread, the space was nearly fully occupied by the newborn bone for the ECAPed Ti group. Moreover, the length of bone-implant contact (as marked by the yellow segment) led a numerous way over that of the CP Ti group. In the follow-up 4 weeks in Figure 9(a,b), a larger cluster of compact bone with more osteons inside can be illustrated and they are interconnected from the cancellous bone zone to the cortical bone
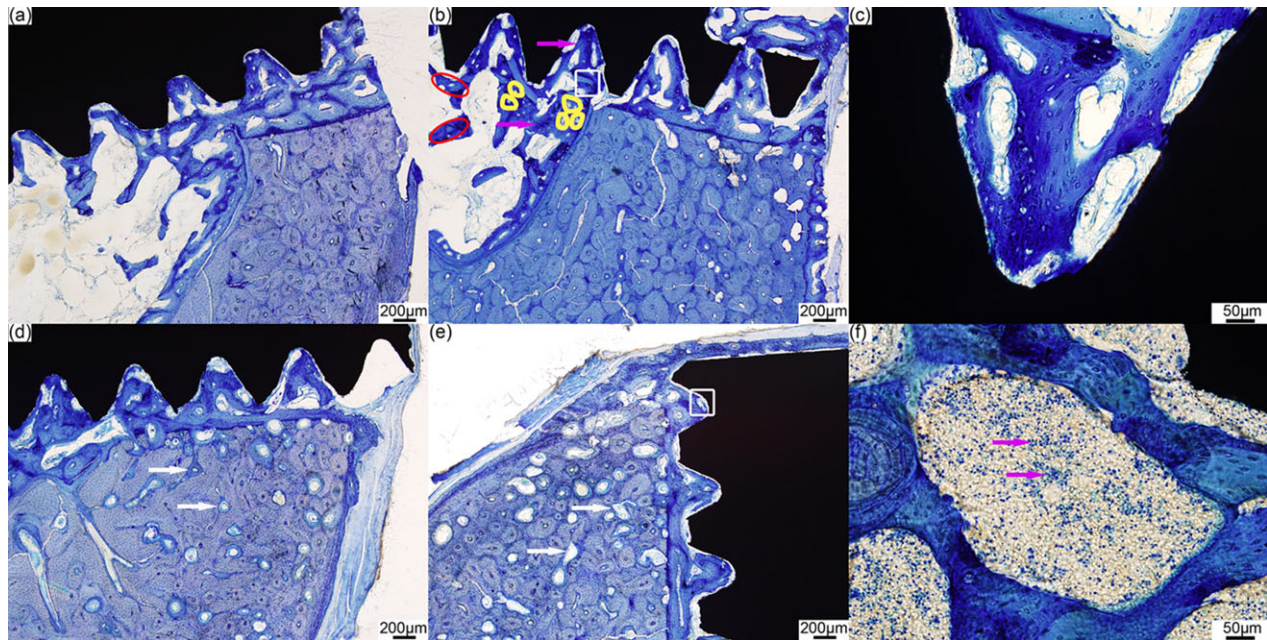

FIGURE 9. Histotomy of bone contact immunostained by toluidine blue at 4 weeks of (a), (b), (c) and 8 weeks of (d), (e), (f), postoperatively. (a) and (d) refers the CP Ti implant; (b) and (e) refers the ECAPed Ti implant; while (c) and (f) refers to the higher-magnification images of (b) and (e). Red arrow and ellipse in (b) represents the lamellar bone. White arrows in (d) and (e) refers to the osteon morphology in the remodeling process. [Color figure can be viewed in the online issue, which is available at wileyonlinelibrary.com.]
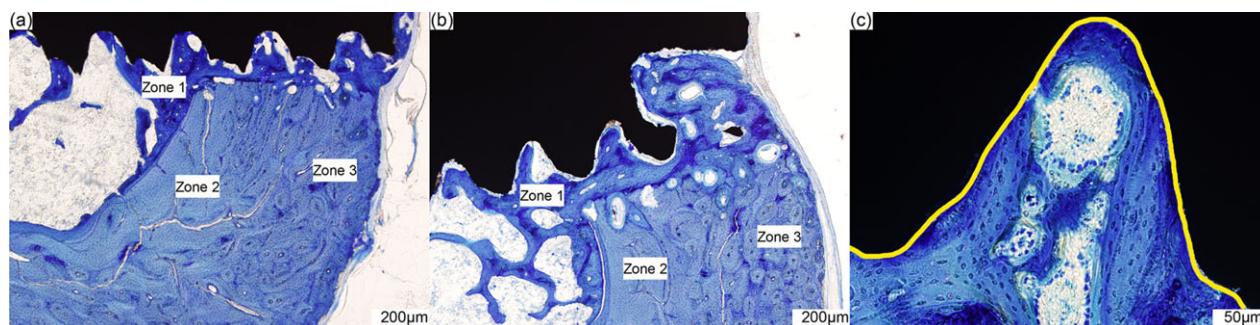
FIGURE 10. Histotomy of bone contact immunostained by toluidine blue at 12 weeks. (a) Refers to the CP Ti implant; (b) refers to the ECAPed Ti implant; while (c) refers to the higher-magnification images of (b). Three different obvious zones of shaped bone were divided in (a) and (b). [Color figure can be viewed in the online issue, which is available at wileyonlinelibrary.com.]

zone, leaving no free room between the implant and the original bone. Especially for the ECAPed Ti group shown in Figure 9(b), an apposition of the newly formed bone could be illustrated on top of the implant necking section. Furthermore, certain hollow cells in the original bone zone in Figure 9(b) revealed the bone transformation itself. While in 8 weeks, this phenomenon of hollow cells in blank become common in Figure 9(d,e) and even the new bone turned to be a little different from the previous form. However, the whole contour was covered by a film of new bone and the density was gradually increased from the outer to the inner space. After 12 weeks implantation, as shown in Figure 10, new bone enveloped the thread of the implants and they were majorly filled in the gap. For the ECAPed Ti group, a phenomenon of the direct bone-implant contact other than the fibrous tissue capsulation against the implant surface can be concluded as a dominant symbol of osseointegration.

DISCUSSION

In-vitro bonelike apatite formation and cell-materials interactions

The attachment and deposition of HA-like compounds on the surface of the ECAPed Ti other than CP Ti after immersion tests reveals well-behaved *in vitro* calcification-a positive reaction between ionic-rich solution and nanostructured surface. An active surface is recognized for the ECAPed Ti since HA formation onto biomaterials even *in vitro* environment is featured as the representative functionality of bioactivity.[23] To further explore the intrinsic mechanism of the different substrates by nature, surface change in composition and component via high-resolution XPS scanning was measured and displayed in the insets in Figure 2(a,b). For both samples, well-defined covalent Ti^{4+} peaks can be typically and clearly discovered in the curve of Ti 2p spectrum. This verifies a TiO_2 film covered on the surface. Meanwhile, featured Ti^0 peak was detected of CP Ti and this implied inert metallic Ti still took up certain percentage on the sample surface. However, no such detection of Ti^0 peak but Ti^{4+} peak was acquired in the case of the ECAPed Ti demonstrated an increasingly high amount of dense and thick oxide layer for nanocrystalline Ti. As for the microcrystalline CP Ti in comparison, an immature

coverage with partial oxide layer on the surface was mixed with tetravalent and nulvalent Ti.

The physics and chemistry feature on the outmost surface due to nanostructured nature is hypothesized as the dominant factor, taking the surface cleavages, energy and chargeability for example, which governs *in vitro* and *in vivo* biological performances. It is known that less impurity and volume deficiencies (such as holes and pits) exists inside the specimen of the ECAPed Ti due to more boundaries and higher energies, which favors smooth surface with little fine deficiency during the grinding friction and small-valued microroughness can be observed in the case of the ECAPed Ti.

It's reported that a correlation with the titanium oxide and bioactivity behaviors including platelet activity was established.[23,24] Thus, bioactive performance of induced HA formation in the present study can be attributed to the oxide component and unique surface structure of the nanostructured ECAPed Ti. In addition, the bioactive property may also refer to another important factor-surface electric charge.

Surface electronegativity of Ti-OH group for conventional Ti in SBF with pH of 7.4 is a long-established knowledge. However, a fresh surface of electropositive and cell-attractive ECAPed Ti due to its nanostructured feature is probably believed to be served to cater the adhesion of negatively charged biomolecule and protein, as described in other works.[25]

The considerable protein adsorption of the ECAPed Ti at the very early stage exhibited a powerful adsorptivity. In the forthcoming period, well-behaved cell adhesion with pronounced amount and stronger spread manner onto the substrates of the ECAPed Ti also showed enhanced *in vitro* capacity of bioaffinity. This can be ascribed to the hydrophilic and active surface, which favors protein and cell adhesion.[26] The ECAPed Ti is exactly born to meet this demand for its matchable downsizing grains with natural nanoscale possessions. The uniform advanced biological performance of the ECAPed Ti could be also attributed to its nanoscale topographic surface, mimicked as the natural surroundings of extracellular matrix (ECM), which provokes the activation and favors the protein attachment.[27]

On the basis of the individual stage on the stepwise interaction between materials and cells,[28] the cytocompatibilities
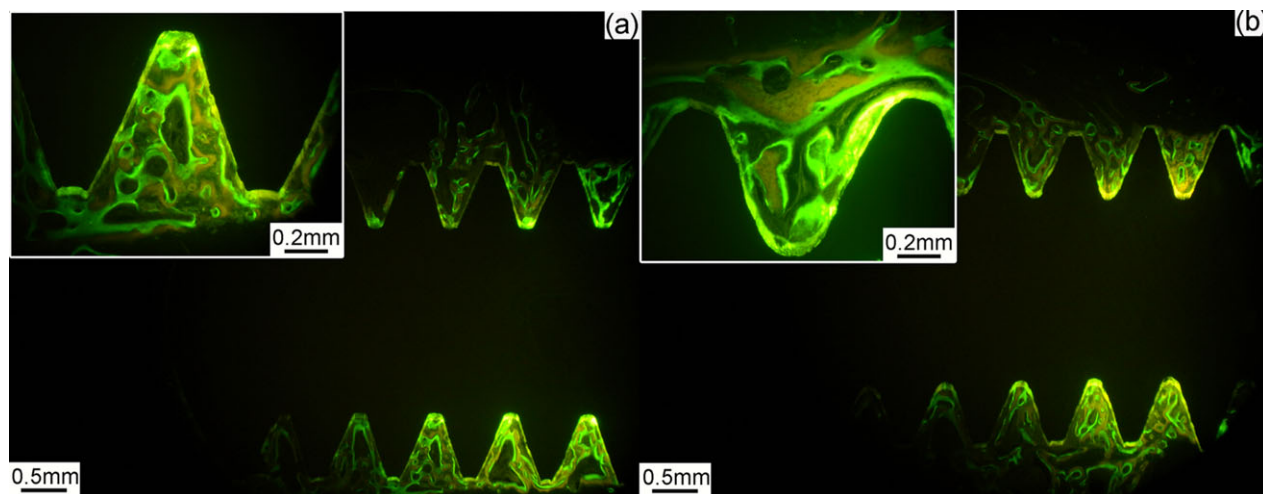
FIGURE 11. Histotomy of bone contact of (a) CP Ti and (b) the ECAP Ti at 4 weeks, illustrated by fluorescence-dyeing reagents, where the yellows reveal the new bone formation of 1-week duration dyed by tetracycline, the pinks reveal the new bone formation of 2-week duration dyed by calcein and the greens reveal that new formation of 4-week duration by calcein-blue. Insets refer to high-magnification images. [Color figure can be viewed in the online issue, which is available at wileyonlinelibrary.com.]

with L929, MG 63, VSMC, and ECV304 were measured in this study. Cell viability results from fibroblast and osteoblast show a totally contrary tendency for the present experimental materials. Preferential attachment and adhesion performance can be clearly observed after several days' culture, according to the results of inhibition in fibroblast and proliferation in osteoblast cell lines. The priority growth in MG63 over L929 also reveals superior bone formation derived from the osteogenous cells, which coincides with the other's work.[26] Even with the different vascular cell lines, experimental samples showed promotion in ECV304 while suppression in VSMC. However, no significant difference in the cell proliferation amongst four types of cell lines can be detected for the ECAPed Ti and CP Ti groups, and it may attribute to the similar extraction components (mainly the metal ions) in an indirect assay way. Taking into consideration of the other stages amid the osteoblast responses with biomaterials, for example, in terms of cell differentiation, there is a comparable outcome between the ECAPed Ti and CP Ti groups during the long-term incubation, and ALP expression in the group of the ECAPed Ti stays a significantly higher level than that in the negative control. Although the release value reflected cell mineralization of the ECAPed Ti is a little higher, there is no significant difference between the ECAPed Ti and CP Ti groups.

Moreover, acellular reaction such as haemocompatibility assessment in Figure 6 displays a low level of hemolysis rate without remarkable difference between the ECAPed Ti and CP Ti groups.

Mechanism of *in vivo* bone growing and remodeling of new bone

Inspired by the intrinsic feature of organic cells (osteons in micron scale) and inorganic apatite component (Ca-P compound in nanodimensional size) as the elementary unit of organ/tissue like bone skeleton, shaped nanotopography was engineered to mimic the circumstances and stimulate the promotion of bone-forming cells as enlightened nature and the predictable sign.[29,30] The nanostructured regime of SPD-induced Ti is also reported to modulate the gene expression and promote the cellular responses *in vitro*.[31] In light of potentially accumulative growth of osteoid bone *in vivo*, osteogenic cells preferentially dominate peri-distributed zone around the substrates with nanoscaled phases.[32] Therefore in this study, the color and structure of newly formed bone are well distinguished from that of autogenous bone aside *in vivo* ever from the initial time point. However at the beginning, the vastly distributive osteocytes as the basic bone-forming cells[33] can be clearly recognized in the neoformed bone under higher-resolution images in Figure 8(c). Hundreds of these osteocytes, densely aggregated and strictly aligned in certain form and shape, perform as the first-step bone formation.[34] Later on after 2 weeks, groups of fresh osteons consisting of concrete cells start to emerge in Figure 8(f), similar to that in the existing bone unit in Figure 8(a). As a result, immature yet intermediate woven bone takes the place of the initially formed spindle-like sparse bone. The osteoinductive interfaces instead of fibrous obstruct between the implant and original bone can be significantly concluded and the replacement procedure proves to be more thoroughgoing and complete in the group of the ECAPed Ti, as shown in Figure 8(e). The growing nature of evolutionary bone continues with the general rules and regulations as time goes on. When it comes to the 4th week, the growth and evolvement of the new bone develops to a stage with the everlasting previous increment of bone density and volume as shown in Figure 7. The bone transformation is almost experienced in progress from the immature bone to the lamellar bone or trabecular [as shown in Fig. 9(b)], with the representative as the mature compact bone. The dynamic procedure of the growing new bone within 4 weeks is recorded in a fluorochrome-marked tracking way. Fluorochrome-dyeing images in Figure 11 record the growth direction and kinetics process of newly formed
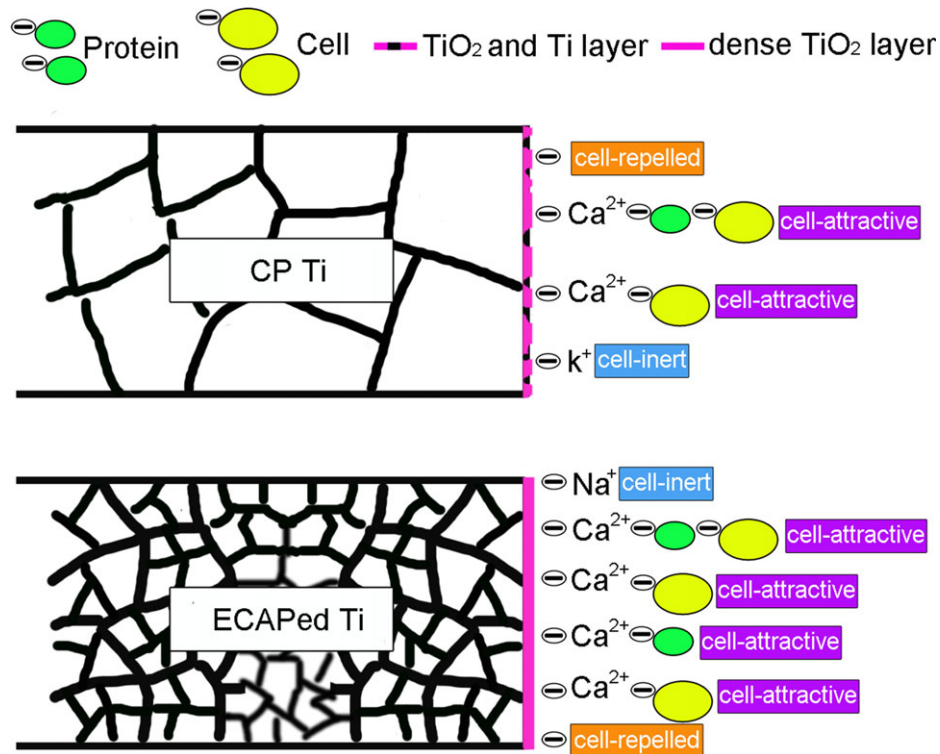
FIGURE 12. Schematic illustration of the proposed mechanism of the interacted surface responses of (a) CP Ti and (b) the ECAPed Ti in the circumstances of SBF, protein and/or *in vitro* or *in vivo* cellular surroundings. [Color figure can be viewed in the online issue, which is available at wileyonlinelibrary.com.]

bone ever since the implantation of materials, during which 4-week duration new bone grows well maturely and burdens the major skeleton with density while 1-week bone starts its outmost formation. Moreover, the ingrowth of neoformed lamellar bone or trabecular alignment are dramatically distinguished without fibrous tissue encapsulation on the interface between bone and the ECAPed Ti implant at 4 weeks (as indicated by the yellow line), which showcases phenomenal osteoinductive integration.

Bone-resorbing cells like osteoclasts with multi-nucleus appeared amidst the bone cells at 8 weeks in Figure 9(f) and it initiated bone resorption, which is also very important in the process of shaping and maturing the new bone.[35] In the follow-up later period, the frame of new bone commenced remodeling itself, bone resorption balanced with bone formation simultaneously, which would also explain the decreasing values of BMD and BV/TV in Figure 7. Talking about the tendency analyzed from the parameters like BMD, the uprising result implies new bone growth and densification (such as osteoid cells) induced by osteoblasts-guided mechanism in the first few weeks, while the downgrading result means a remodeling process of bone from newly-formed immature bone (woven bone) to mature substitute (lamellar bone), which is usually driven by multi-nucleated osteoclasts. Another finding from Figure 7(a) is that a rising peak of BMD till 8 weeks can be observed in the targeted zone around CP Ti, while this peak of bone-growing turns left toward 4 weeks in that around the ECAPed Ti. This left-shift reveals a fast recovery and

promising bone-healing in a much shorter time due to the rapid growth and mature transformation of new bone. Together with the phenomenon of fibrous-free interface and osseointegration when bone contacted with ECAPed Ti, a totally different bone formation mechanism from that for the conventional CP Ti would be proposed. Till the end of implantation at 12 weeks, three divided zones of bone in different shape can be detected. Remodeling achievement is mostly finished in the case of the ECAPed Ti from the parts like bone marrow cavity, inner and outer zone of the cortical bone part. It is hypothesized that nanostructured Ti stimulates the fast ingrowth of bone-forming cells and follow-up remodeling process toward the implant when they are interacted. A full envelop of direct bone contact encapsulated onto the implant is clearly identified as the desirable osseointegration after rapid involvement of highly-motivated osteoclasts over balanced osteoblasts participation, leaving no time and room for fibrous tissue activation as shown in Figure 10.

Together with the XPS analysis discovered in our study, a schematic description of the proposed mechanism is illustrated in Figure 12. The dominant component of the thick and flawless layer of TiO_2 is obviously discriminated, which is strongly dependent on the different grain sizes, microcrystalline or nanocrystalline. Because of the capacity of electronegativity derived from such densely TiO_2 layer or active external hydroxy in the case of the nanocrystalline ECAPed Ti, cations of different types in the near circumstances were captured and neutralized. As for those partially

neutralized cation like calcium (Ca), there is enough room for the negatively charged biomolecule such as proteins or cells to bone together, providing a precursor of the follow-up tissue generation even skeleton formation. Such pronounced bioactive phenomenon was found in the group of the ECAPed Ti with exterior active layer and interior nanostructures. While for those fully neutralized and bonded cations like sodium (Na) or potassium (K), it keeps substrates repellent or inert onto the cells or biomolecule, most of which is also electronegative. Inferior cell-attractive surface of the microcrystalline CP Ti with the covered mixture of bare metallic Ti and TiO_2 brings about less bioaffinity than that of the nanocrystalline ECAPed Ti.

CONCLUSIONS

In summary, the nanocrystalline pure titanium (ECAPed Ti) in the present study has shown an improved combination of not only the *in vitro* bioactivity, bioaffinity, and long-term cellular functionalization in cytobiology, but also the *in vivo* biostability and humanized bio-osseointegration in histomorphology. Deposition of bonelike apatite on the substrate of the ECAPed Ti is unprecedented observed under the static immersion in the natural SBF environment. Meanwhile, the less rough surface with more hydrophilicity of the ECAPed Ti up-regulates protein adsorption, cell proliferation and follow-up differentiation and mineralization to some extent. Correspondingly, tailored ECAPed Ti with the nanostructured grains concretely avails osseointegration, thus enhances the quick bone-formation and fast recovery after the rapid growth and remodeling of the newly formed bone. Therefore, besides its widespread application in aerospace, automotive and sport goods fields, bulk nanostructured titanium with leading bioactivity and fast bone regeneration can be actively and intelligently engineered to meet the extended function in life innovation industry on demand.

ACKNOWLEDGMENTS

REFERENCES

1. Williams DF. Biocompatibility of Clinical Implant Materials. Boca Raton: CRC Press;1981.
2. Brunette DM, Tengvall P, Textor M, Thomsen P. Titanium in Medicine. New York: Springer-Verlag Berlin Heidelberg;2001.
3. Legeros RZ, Craig RG. Strategies to affect bone remodeling: osteointegration. J Bone Miner Res 1993;8:S583–S586.
4. Qazi JI, Rack HJ. Metastable beta titanium alloys for orthopedic applications. Adv Eng Mater 2005;7:993–998.
5. Narita K, Niinomi M, Nakai M, Akahori T, Tsutsumi H, Oribe K, et al. Mechanical properties of implant rods made of low-modulus β-type titanium alloy, Ti-29Nb-13Ta-4.6Zr, for spinal fixture. J Japan Inst Metals 2008;72:674–678.
6. Khang D, Lu J, Yao C, Haberstroh KM, Webster TJ. The role of nanometer and sub-micron surface features on vascular and bone cell adhesion on titanium. Biomaterials 2008;29:970–983.
7. Kim HW, Koh YH, Li LH, Lee S, Kim HE. Hydroxyapatite coating on titanium substrate with titania buffer layer processed by sol–gel method. Biomaterials 2004;25:2533–2538.
8. Liu YL, Enggist L, Kuffer AF, Buser D, Hunziker EB. The influence of BMP-2 and its mode of delivery on the osteoconductivity of implant surfaces during the early phase of osseointegration. Biomaterials 2007;28:2677–2686.
9. Valiev RZ. Nanostructuring of metals by severe plastic deformation for advanced properties. Nat Mater 2004;3:511–516.
10. ISO-286:1988, ISO system of limits and fits-Part 2: Tables of standard tolerance grades and limit deviations for holes and shafts. IHS, Switzerland (2006).
11. Valiev RZ, Semenova IP, Latysh VV, Rack H, Lowe TC, Petruzelka J, et al. Nanostructured titanium for biomedical applications. Adv Eng Mater 2008;10:B15–B17.
12. Semenova IP, Korshunov AI, Salimgareeva GK, Latysh VV, Yakushina EB, Valiev RZ. Mechanical behavior of ultrafine-grained titanium rods obtained using severe plastic deformation. Phys Metals Metallography 2008;106:211–218.
13. Valiev RZ, Langdon TG. Principles of equal-channel angular pressing as a processing tool for grain refinement. Prog Mater Sci 2006;51:881–981.
14. Park JW, Kim YJ, Park CH, Lee DH, Ko YG, Jang JH, et al. Enhanced osteoblast response to an equal channel angular pressing-processed pure titanium substrate with microrough surface topography. Acta Biomaterialia 2009;5:3272–3280.
15. Estrin Y, Ivanova EP, Michalska A, Truong VK, Lapovok R, Boyd R. Accelerated stem cell attachment to ultrafine grained titanium. Acta Biomaterialia 2011;7:900–906.
16. Truong VK, Lapovok R, Estrin YS, Rundell S, Wang JY, Fluke J, et al. The influence of nano-scale surface roughness on bacterial adhesion to ultrafine-grained titanium. Biomaterials 2010;31:3674–3683.
17. Lee S, Choi J, Shin S, Im YM, Song J, Kang SS, et al. Analysis on migration and activation of live macrophages on transparent flat and nanostructured titanium. Acta Biomaterialia 2011;7:2337–2344.
18. ASTM-G31-72: Standard practice for laboratory immersion corrosion testing of metals Annual Book of ASTM Standards, Philadelphia, PA (2004).
19. Nie FL, Zheng YF, Wei SC, Hu C, Yang G. In vitro corrosion, cytotoxicity and hemocompatibility of bulk nanocrystalline pure iron. Biomed Mater 2010;5:065015.
20. Nie FL, Wang SG, Wang YB, Wei SC, Zheng YF. Comparative study on corrosion resistance and in vitro biocompatibility of bulk nanocrystalline and microcrystalline biomedical 304 stainless steel. Dental Mater 2011;27:677–683.
21. Stolyarov VV, Zhu YT, Alexandrov IV, Lowe TC, RZ Valiev. Influence of ECAP routes on the microstructure and properties of pure Ti. Mater Sci Eng A 2001;299:69–67.
22. Semenova IP, Salimgareeva GK, Latysh VV, Valiev RZ. Enhanced fatigue properties of ultrafine-grained titanium rods produced using severe plastic deformation. Solid State Phenomena 2008;140:167–172.
23. Hench LL, Wilson J. Surface-active biomaterials. Science 1984;226:630–636.
24. Wen M, Gu JF, Liu G, Wang ZB, Lu J. Nanocrystalline titanium to mesoporous anatase with high bioactivity. Crystal Growth Design 2007;7:2400–2403.
25. Att W, Hori N, Takeuchi M, Ouyang J, Yang Y, Anpo M, et al. Time-dependent degradation of titanium osteoconductivity: An implication of biological aging of implant materials. Biomaterials 2009;30:5352–5363.
26. Faghihi S, Zhilyaev AP, Szpunar JA, Azari F, Vali H, Tabrizian M. Nanostructuring of a titanium material by high-pressure torsion improves pre-osteoblast attachment. Adv Mater 2007;19:1069–1073.
27. Rani VVD, Manzoor K, Menon D, Selvamurugan N, Nair SV. The design of novel nanostructures on titanium by solution chemistry for an improved osteoblast response. Nanotechnology 2009;20:195101.

28. Mendonca G, Mendonca DBS, Aragao FJL, Cooper LF. Advancing dental implant surface technology-From micron- to nanotopography. Biomaterials 2008;29:3822–3835.

29. Dvir T, Timko BP, Kohane DS, Langer R. Nanotechnological strategies for engineering complex tissues. Nat Nanotechnol 2011;6: 13–22.

30. Molly MS, George JH. Exploring and engineering the cell surface interface. Science 2005;310:1135–1138.

31. Faghihi S, Azari F, Zhilyaev AP, Szpunar JA, Vali H, Tabrizian M. Cellular and molecular interactions between MC3T3-E1 pre-osteoblasts and nanostructured titanium produced by high-pressure torsion. Biomaterials 2007;28:3887–3895.

32. Webster TJ, Ejiofor JU. Increased osteoblast adhesion on nano-phase metals: Ti, Ti6Al4V, and CoCrMo. Biomaterials 2004;25: 4731–4739.

33. Yu XW, Xie XH, Yu ZF, Tang TT. Augmentation of screw fixation with injectable calcium sulfate bone cement in ovariectomized rats. J Biomed Mater Res Part B: Appl Biomater 2009;89:36–44.

34. Wang YB, Xie XH, Li HF, Wang XL, Zhao MZ, Zhang EW, et al. Biodegradable CaMgZn bulk metallic glass for potential skeletal application. Acta Biomaterialia 2011;7:3196–3208.

35. Missbach M, Jeschke M, Feyen J, Muller K, Glatt M, Green J, et al. A novel inhibitor of the tyrosine kinase Src suppresses phosphorylation of its major cellular substrates and reduces bone resorption in vitro and in rodent models in vivo. Bone 1999;24:437–449.